 CMC, vol.39, no.1, pp.21-47, 2014

Change of Scale Strategy for the Microstructural Modelling of Polymeric Rohacell Foams

J. Aubry[1], P. Navarro[1], S. Marguet[1], J.-F. Ferrero[1], O. Dorival[2], L. Sohier[3] and J.-Y. Cognard[3]

Abstract: In this paper a numerical model dedicated to the simulation of the mechanical behaviour of polymeric Rohacell foams is presented. The finite elements model is developed at the scale of the microstructure idealized by a representative unit cell: the truncated octahedron. Observations made on micrographs of Rohacell lead to mesh this representative unit cell as a lattice of beam elements. Each beam is assigned a brittle linear elastic mechanical behaviour in tension and an elasto-plastic behaviour in compression. The plasticity in compression is introduced as a way to mimic the buckling of the edges of the cells observed in experimental crushing tests. A contact law introduced between the beams stands for densification. A change in scale is then realized by increasing the length of the edges of the unit cell. Several computations show the ability of the proposed approach to preserve the physical degradation phenomena and the loads while drastically decreasing the computational time.

Keywords: Rohacell foam, mechanical behaviour, microstructure, change of scale strategy

1 Introduction

This paper is about the modelling of the mechanical behaviour of Rohacell polymeric foams. These polymetacrylimid foams are closed cells foams from [Evonik (2011)]. Their typical microstructure is displayed in Fig. 1. It includes several types of randomly distributed irregular polyhedra made of plastic.

[1] Université de Toulouse, Institut Clément Ader (ICA), UPS, ISAE, INSA, Mines d'Albi, 135 avenue de Rangueil, F-31077 Toulouse, France

[2] LMT-Cachan, (ENS Cachan / Université Paris 6 / C.N.R.S.), 61 avenue du Président Wilson, 94230 Cachan, France

[3] Université de Bretagne Occidentale, Laboratoire Brestois de Mécanique et des Systèmes (LBMS), ENSTA Bretagne, 2 rue François Verny, 29806 Brest Cedex 9, France

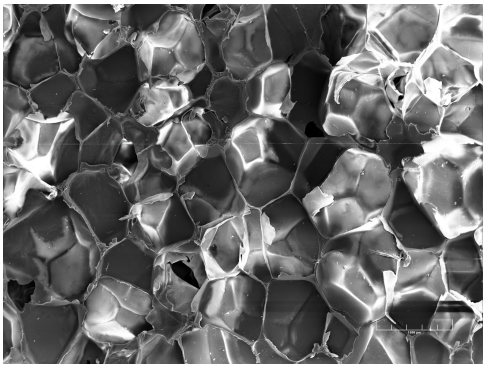

Figure 1: SEM micrography: microstructure of the Rohacell 51A foam

Rohacell foams are widely used as a core material for sandwich structures. These structures are, for example, well suited for aeronautic constructions where high levels of stiffness and strength are needed with a minimal associated mass.

However, composite sandwich structures are very sensitive to out-of-plan loadings, like impacts. [Tawk, Aubry, Navarro, Ferrero, Marguet, Rivallant, Lemaire and Rauch (2012); Navarro, Aubry, Marguet, Ferrero, Lemaire and Rauch (2012a)] have studied the effects of oblique impacts on sandwich structures made of two plies of glass fibres/epoxy resin woven fabrics and 20 mm thick Rohacell 51A foam. The impactor, a steel ball of mass 28 g and diameter 19 mm, is launched at the velocity of 65 m/s with an angle of 15° relative to the upper skin. The resulting degradations are displayed in Fig. 2.

The area of damaged foam is spread on a larger zone than the damaged skin one. The major degradation phenomena are of two natures: crushing below the path of the impactor and coupled crushing and shear around this crushed zone. These damages lead to the separation of the foam and the skin. As a result the skin is not stabilized anymore and becomes free to bend and buckle. The bending then induces the tensioning of the fibres, leading to their brittle failure as observed by [Navarro, Aubry, Marguet, Ferrero, Lemaire and Rauch (2012b)].

Therefore, despite its relatively low mechanical properties and density, the foam plays a major role on the strength of the sandwich structure ([Schubel, Luo and Daniel (2007)]). Being able to accurately predict its failure is essential for the design process.

Generally, two main strategies are used to model this kind of materials: continuous and discrete models.

Figure 2: Degradation of a sandwich structure after oblique impact

In the continuous approach, the idea is to associate a simple continuous mesh with a complex homogenized constitutive material law. One way to introduce the degradations is to define a yield criterion in the material law to deal with the plateau observed in the crushing of foams as was proposed by [Abrate (2008)]. This is most of the time performed in the (hydrostatic pressure, Cauchy stress) space. Most of commercial finite elements codes offers this kind of material laws ([Simulia (2011); Altair (2009)]). Another way, used by [Azikri de Deus and Alves (2009)], consists in the use of an elasto-visco-plastic law in which a term depending on the volumetric strain is added to compute the hydrostatic pressure. In order to deal with the compaction step, [Aktay, Johnson and Kröplin (2008); Aktay, Johnson, Toksoy, Kröplin and Güden (2008)] have associated SPH formulations to classic three dimensional finite elements. The idea is to replace crushed elements subjected to huge strains with particles. Another strategy, proposed by [Bishay and Atluri (2012); Bishay and Atluri (2013)], consists in developing continuous finite elements that can intrinsically represent the microstructure. The authors have developed several Voronoi cell finite elements to build fine descriptions of heterogeneous microstructures. This approach has shown a good capability to predict the behaviour of complex materials under a wide variety of physical phenomena [Dong and Atluri (2013); Bishay and Atluri (2014)]. To summarize, continuous approaches offer: simple geometries and attractive computational times at the cost of a complex homogenized material law, farther from the physics than discrete models.

In the discrete approach, a mesh as close as possible to the real microstructure

is associated to a simple constitutive mechanical behaviour law. The underlying idea is that the geometry of the microstructure is predominant over the mechanical behaviour of the plastic in the macroscopic response of the foam. Many studies deal with this kind of modelling. They rely on the use of an idealized microstructure which can come from experiments or from mathematical constructions based on polyhedra. For instance, [Gaitanaros, Kyriakides and Kraynik (2012)] have used X-ray tomography on opened cells foam associated with Brakke's Surface Evolver [Kraynik, Reinelt and van Swol (2003)] to investigate the mechanical behaviour of aluminium foams. The authors have paid particular attention to the random distribution of the microstructure and to the geometry of the edges. [Laroussi, Sab and Alaoui (2002)] have used a microstructure based on truncated octahedron to investigate the yield surface of open cells foams related to the buckling of the edges. All the aforementioned discrete models are well suited to understand the physics that drives the response at the macroscopic scale. However, they generally induce a huge computational time directly related to the fine description of the microstructure.

In this study, a new modelling of Rohacell foams is proposed for impact applications. It is developed using the finite elements method with explicit time integration scheme and relies on a simplified description of the microstructure and material law described in section 2. The identification of the model is achieved on three proposed scales in section 3. Finally, the ability of the model to preserve the physical degradation phenomena and load transfer while drastically decreasing the computational time is discussed in section 4.

2 Modelling strategy

This section starts with a short review of the macroscopic behaviour of Rohacell foams. The modelling strategy is then detailed. It aims at building a model usable at macroscopic scales and relies on several "pragmatic" assumptions which are compromises between the micro and macro scales.

2.1 Macroscopic behaviour of Rohacell foams

The physical phenomena involved in the mechanical behaviour of polymeric foams such as Rohacell are now well known and a comprehensive review is available in [Gibson and Ashby (2001)].

In tension, a specimen S made of Rohacell foam exhibits a brittle linear elastic response characterized by a macroscopic elasticity modulus E^S and by a tensile failure stress $\sigma^{S,tf}$.

In compression, after a short linear elastic part (modulus E^S), the elastic buckling of

the cells initiates a plateau stress of value $\sigma^{S,y}$. The edges and walls of the cell start to buckle in a localized zone that propagates through the thickness of the specimen. Once the crushing strain is raised to a critical level ($\varepsilon_{S,d}$), the material accumulates and densification occurs.

In shear, a specimen of Rohacell foam exhibits a linear elastic response up to the failure. The associated elasticity modulus and shear failure stress are G_S and $\sigma^{S,sf}$ respectively. If the shear specimen has a sufficient length / height ratio (12 according to [ASTM Standard (2011)]), tensile failure initiates in the principal tensile stress direction: the tensile behaviour drives the failure in shear.

A synthesis of the typical target values borrowed from the data-sheets of the manufacturer [Evonik (2011)] is given in Tab. 1.

Table 1: Typical properties of Rohacell polymeric foams from [Evonik (2011)]

Property	Value	Unit
Density ρ^S	around 52	kg/m^3
Elastic modulus E^S	70 - 75	MPa
Shear modulus G^S	19 - 24	MPa
Compressive strength $\sigma^{S,y}$	0.7 - 0.9	MPa
Tensile strength $\sigma^{S,tf}$	1.6 - 1.9	MPa
Shear strength $\sigma^{S,sf}$	around 0.8	MPa

These values are used in section 3 for the identification process.

2.2 Unit cell

As presented earlier in Fig. 1, Rohacell foams present a closed bubble shaped microstructure. Several options are available to generate a representative mesh of this microstructure. [Gibson and Ashby (2001)] propose various arrangements of cubes to distribute the material. [Okabe, Boots, Sugihara and Chiu (2000)] report the importance of Voronoi's cells in nature. Voronoi's cells form a partition of space by area of influence. They seem to be well suited for modelling phenomenon with variability but are quite complex to build [Dong and Atluri (2012a); Dong and Atluri (2012b)]. [Jang, Kraynik and Kyriakides (2008)] use a more sophisticated approach which relies on the simulation of the growing process of the bubbles of polymeric foam by including the superficial tension effects.

In this paper, the retained approach is chosen as a compromise between representativeness of the microstructure and simplicity. The microstructure is obtained from one single cell: the truncated octahedron as was proposed by [Zhu, Knott and Mills

(1997); Laroussi, Sab and Alaoui (2002); Gong and Kyriakides (2005); Gong, Kyriakides and Jang (2005)]. This semi-regular polyhedron is one of the five plotted in Fig. 3 able to pave the whole 3D space ([Thomson (1887)]).

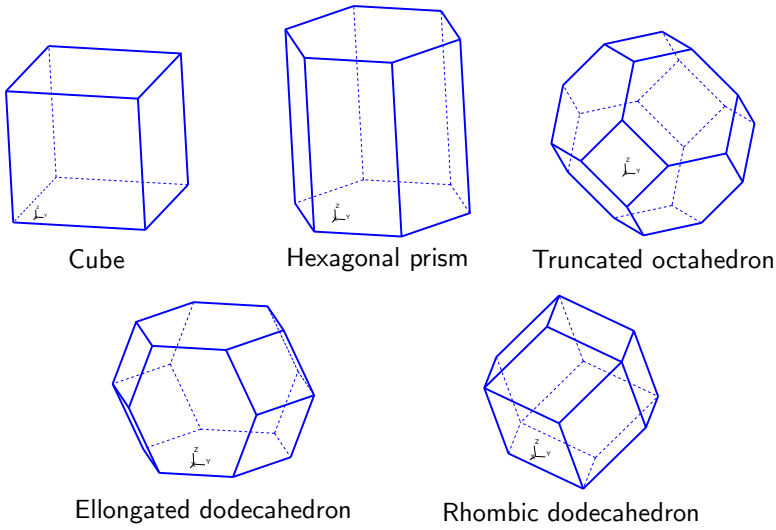

Figure 3: Polyhedra able to pave the 3D space

Only two polyhedra from Fig. 3 present an orthotropic geometry: the cube and the truncated octahedron. Since the truncated octahedron is the only one of them to offer a shape that matches the shape of the bubbles of Rohacell foam, it appears to be the best candidate for the elementary cell of the mesh. This is the first main simplification of the proposed model.

Once the geometry of a unit cell selected, a suited type of finite element has to be chosen. The truncated octahedron includes 24 vertex, 36 edges and 14 faces: 6 squares and 8 hexagons. The second main simplification arises from the material distribution in the microstructure. It can be seen from Fig. 4, that most of the plastic is concentrated in the nearly straight edges and nodes of the cells. The remainder constitutes the walls that link the edges ([Gibson, Ashby and Harley (2010); Gaitanaros, Kyriakides and Kraynik (2012)]). This observation, in agreement with [Li, Mines and Birch (2000)], can also be done for Nomex® honeycomb cores where, due to surface tensions, the resin concentrates in the vertical straight edges ([Gornet, Marguet and Marckmann (2006); Aminanda, Castanié, Barrau and Thevenet (2009)]). As a result, the walls of the cell are neglected in the proposed model. Only one dimensional elements are used.

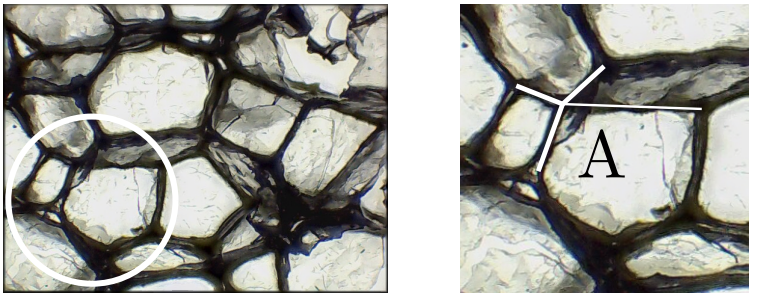

Figure 4: Optical micrography: predominance of edges over walls in Rohacell

To choose between truss and beam elements, rotations must be considered. In the microstructure, each vertex is most often in link with 4 other vertex (see point A in Fig. 4). The accumulation of plastic at each vertex makes it difficult to rotate freely. In other words, if an edge rotates, it will induce a moment on the other connected edges. Hence, beam elements appear to be more suitable to take into account this effect of constrained rotations. The linear 2 nodes Timoshenko beam element B31 of the Abaqus finite element code is used to build the mesh ([Simulia (2011)]).

In terms of cross-section of the beams, the use of a circular shape is retained. This is of course a simplification over the observed cross-sections on micrographs which look more triangular than circular ([Gong, Kyriakides and Jang (2005)]). This choice is done for two reasons: it avoids the definition of an oriented local frame for each beam and it greatly simplifies the contact between the beams when densification occurs. Two radii are associated to the beam elements: the effective and the contact ones. The effective radius is used to compute the stiffness of the finite beam element. The contact radius stands for densification. It enables to end the plateau step at the suited strain by driving the initiation of the contact between beam elements.

To finalize the description of the unit cell, the length a of the edge has to be selected. [Li, Mines and Birch (2000)] have performed statistics upon the microstructure of Rohacell foam. They have found a mean length $a = 0.25$ mm which is used in this study as the "true" length.

However, for a given volume of structure, the number of cells involved in the mesh is proportional to a^3. This can quickly lead to a very high number of degrees of freedom in the finite element model. Therefore, the proposed change in scale strategy simply relies on an artificial increase of the length a of the edge. In the following, it is shown that this approach can be used at various scales ($a = 0.25, 0.5$

and 1 mm) with convincing results. Thus, the choice of the edge length a becomes a compromise between the size of the structure, the details the engineer wants to capture and the computational cost.

2.3 Constitutive mechanical behaviour

Here, the mechanical behaviour of the beam is discussed. The true stress versus true strain curve presented in Fig. 5 is injected into the beam elements.

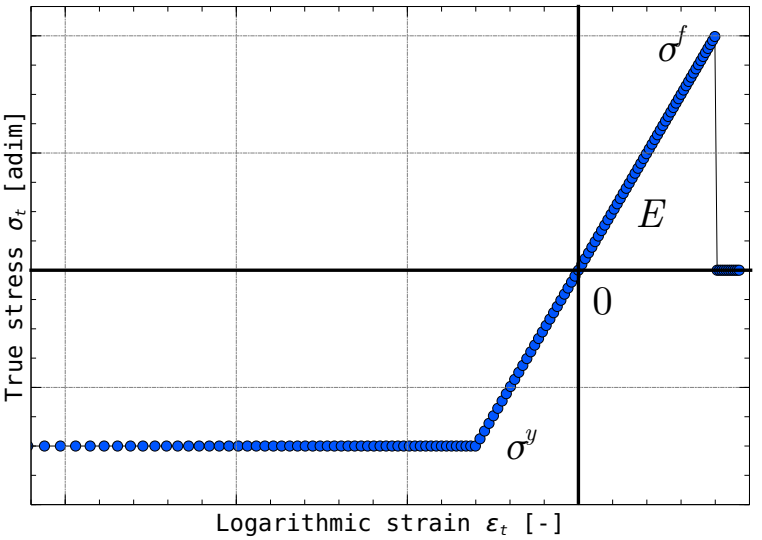

Figure 5: Mechanical behaviour law introduced into the beam elements

In tension and shear, the response is linear elastic of modulus E and Poisson's coefficient ν. A brittle failure stress σ^f in used in tension to break the beams. In compression, an elasto-perfectly plastic behaviour is employed to mimic the elastic buckling of the edges of the foam which drives the plateau stress when crushing occurs. The associated yield stress is noted σ^y.

2.4 Mesh generation

Up to now, only one single perfect elementary cell has been considered. The generation of a part made of Rohacell foam is performed in three steps: generation of a parallelepipedic mesh of perfect cells; perturbation of the generated mesh to

introduce variability and isotropy; bounding of the perturbed mesh to the suited shape.

A program written in the Python programming language and using the Parallel-Python library has been developed and used on a massively parallel infrastructure with both shared and distributed memory.

2.4.1 Generation of a parallelepipedic mesh

The first step simply relies on translations of the reference unit cell in the three directions of the space. The inputs of the procedure are: the length a of the unit cell, the number of required cells in the x, y and z directions.

2.4.2 Perturbation of the generated mesh

This second step introduces variability in the model by moving the nodes according to a Gaussian distribution. Each node of the model is shifted with a perturbation displacement vector computed as follows:

1. Two angles ϕ and θ are drawn with equiprobability by step of $1°$: ϕ between $0°$ and $360°$ and θ between $0°$ and $180°$. They define the translation unit vector of the node.

2. Then, a distance da following a Gaussian distribution law of mean value $\mu = 0$ and standard deviation σ_{sd} - which has to be chosen carefully - is randomly chosen.

Once the perturbation vector is computed, the new coordinates of the node are updated as displayed in Fig. 6.

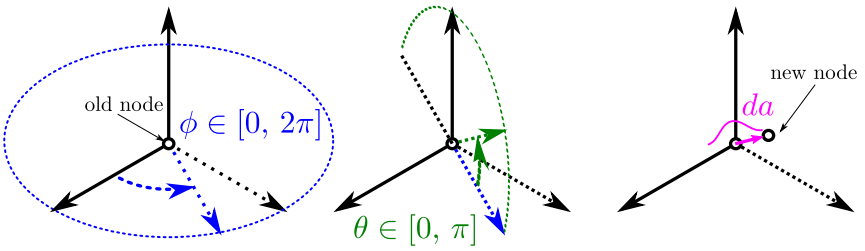

Figure 6: Perturbation of nodes: illustration of the algorithm

The standard deviation σ_{sd} is computed in order to obtain a quasi-isotropic mechanical behaviour of a representative volume element of the microstructure. As

mentioned in [Jang, Kyriakides and Kraynik (2010)], due to the manufacturing process, most of the foams exhibits some anisotropy in their rise direction. Hence, the proposed strategy should be enriched in the future to deal with this point (by stretching the mesh in one direction for example). As can be seen on the left of Fig. 7, five preferential directions can be extracted from a single unit cell.

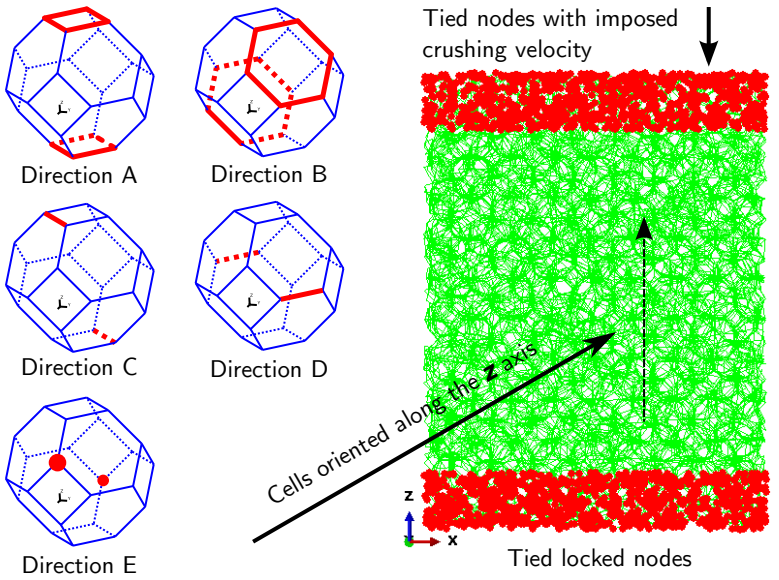

Figure 7: Preferential directions of a single truncated octahedron unit cell

Directions A and B are respectively orthogonal to a square and to a hexagonal face of the unit cell. Direction C links the opposite edges of the unit cell located at the intersection of a square and a hexagonal face. Direction D does the same thing for the edges located at the intersection of two hexagonal faces and direction E is oriented by two opposite points located at the intersection of two hexagonal and one square faces.

To determine the standard deviation σ_{sd} parameter for the mesh perturbation, a cube of edge length l at least equal to twenty times the length of a unit cell edge a ($l \geq 20\,a$) is filled with a perturbed microstructure (Fig. 7b). The ratio $k = l/a \simeq 20$ is determined empirically by running several simulations while varying the number of cells in each direction. $k = 20$ results in at least 12 cells in each direction which is enough to have a homogenized behaviour. Five cubes are generated: one per preferential direction. For each of them, the preferential direction is aligned with

the z direction of the cube as displayed on the right of Fig. 7. The five cubes are then crushed numerically in the z direction and the macroscopic load versus displacement curves are extracted from the results. The simulations are performed with the finite elements software Abaqus (Explicit module). The procedure is repeated with various σ_{sd} parameters until a variation less than 15 % is obtained between the five stress versus strain curves (in terms of elastic modulus and plateau stress). An illustration is given in Fig. 8 for a cube of edge length $l = 6$ mm, a unit cell of length $a = 0.25$ mm and arbitrary material characteristics.

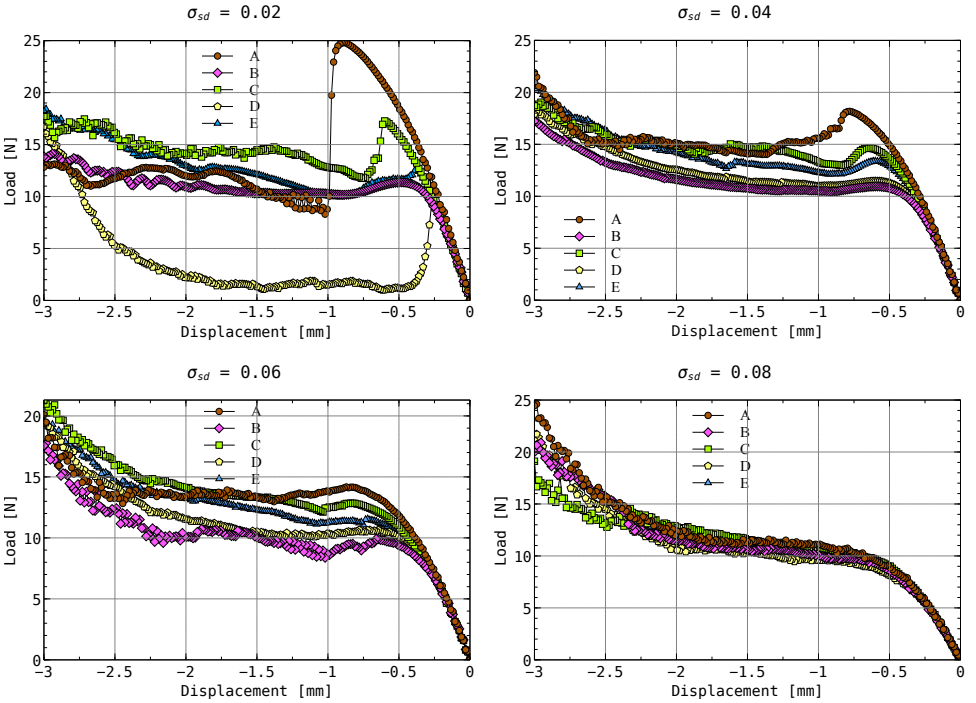

Figure 8: Study of the influence of the standard deviation parameter σ_{sd} on the isotropic nature of the mechanical behaviour

With this methodology, the mechanical behaviour of the microstructure can be considered as quasi-isotropic. This is an assumption over the anisotropy of a real foam that exhibits a slightly different mechanical behaviour in its rise direction. The values of σ_{sd} for the three cell sizes are given in Tab. 3.

Fig. 9 gives an illustration of the distribution of the edge lengths for the three meshes. In this plot it can be noticed that the minimal length a_{min} of the mesh can not be less than one fifth of the mean length a. This is done arbitrarily to avoid too small elements that penalize the calculation time.

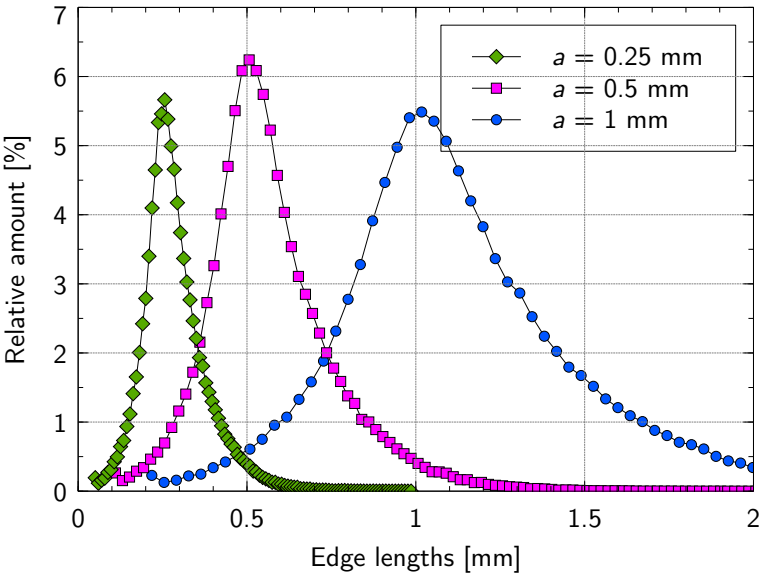

Figure 9: Distribution of the edges length for typical meshes obtained with a =0.25, 0.5 and 1 mm

2.4.3 Bounding to the suited shape

At this stage, a parallelepipedic block of perturbed cells has been generated. This last step consists in rebounding this block. In a first time, the domain corresponding to the suited shape is meshed with tetrahedra. The position of each node of the initial foam mesh is checked to determine if the node belongs to a tetrahedron or not. Two groups of nodes are then created : the inside nodes and the outside ones. The beam elements made of two outside nodes are deleted whereas the beam elements made of two inside nodes are retained. The beam elements constituted of one inside node and one outside node are subjected to a special treatment. For each of them, the outside node is projected on the boundary of the domain, along the direction of the element. At the end, all the nodes of the mesh are either inside nodes, either border nodes. An illustration of what can be done is given in Fig. 10.

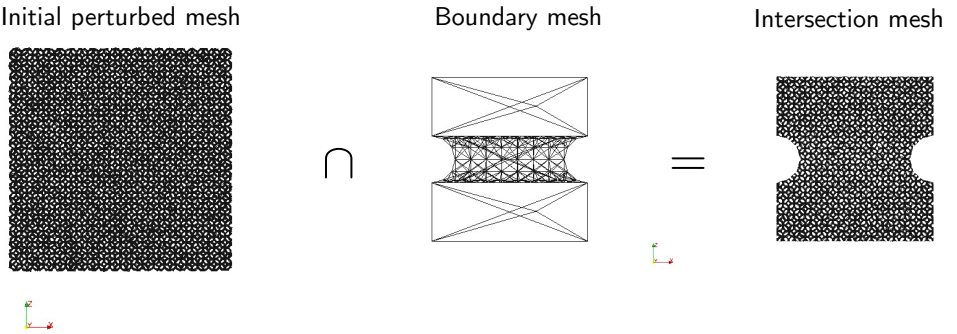

Figure 10: Rebounding step: example of a tensile test specimen

The generation of a part made of Rohacell foam is now over. In the next session, the identification process of the value of the parameters of the model is discussed.

3 Identification

In this part the parameters of the model are obtained by inverse identification. For reminder, these parameters are: a the length of the edge of the perfect unit cell, ρ the density of the plastic, E the elastic modulus, ν the Poisson's coefficient, σ^f the failure stress in tension, σ^y the yield stress in compression, r the radius of the beam elements and r^c the radius of contact between the beam elements.

The starting point of the identification process is the choice of the lengths a of the edges of the unit cell. In order to introduce the change in scale strategy, three values are retained, evolving from the "real" value $a = 0.25$ mm to $a = 1$ mm with an intermediate value of 0.5 mm.

For each of these three values of a, the elastic modulus and the Poisson's coefficient are taken equal to $E = 3\,000$ MPa and $\nu = 0.3$. These values are chosen to represent the elastic characteristics of polymetacrylimid. This choice is not critical since it only shifts the other parameters without impacting the physics.

Before describing the next steps, it has to be recalled that the model is developed for the simulation of impact loadings on sandwich structures in the context of the finite elements method associated with explicit time integration scheme. As the computational time can rapidly become important for the smallest microstructure, an imposed strain rate of $\dot{\varepsilon} = 200\ \mathrm{s}^{-1}$ is applied to the specimen for the identification process.

The identification procedure makes use of virtual parallelepipedic specimens whose

dimensions and loading conditions are listed in Tab. 2. An illustration of the shapes of the meshes is displayed in Fig. 17 (shapes only, no sizes).

Table 2: Computations for identification

	tensile		compressive	shear	tie length b
a	quasi-static	$\dot{\varepsilon} = 200\ \mathrm{s}^{-1}$	$\dot{\varepsilon} = 200\ \mathrm{s}^{-1}$	$\dot{\varepsilon} = 200\ \mathrm{s}^{-1}$	
0.25	$6 \times 6 \times 8$ mm		$6 \times 6 \times 8$ mm	$72 \times 6 \times 8$ mm	2×1 mm
0.5	$12 \times 12 \times 16$ mm		$12 \times 12 \times 16$ mm	$144 \times 12 \times 16$ mm	2×2 mm
1	$24 \times 24 \times 32$ mm		$24 \times 24 \times 32$ mm	$288 \times 24 \times 32$ mm	2×4 mm

Tensile and compressive specimens are cubes involving at least 12 cells in each direction as mentioned in subsection 2.4.2. The shape of the shear specimens is chosen to present a length / height ratio equal to 12 in agreement with the C 273 specifications of [ASTM Standard (2011)].

The identification of the parameters then follows the steps:

1. The radius r of the beam elements is determined from a quasi-static tensile virtual test of a cube of Rohacell. In this model, the material law is linear elastic and the only prerequisites are E, ν and the mesh. A first computation is done with an arbitrary radius r. The value of the radius r is adjusted to match the computed macroscopic modulus with the value E^S given in Tab. 1.

2. The density ρ of the material is then computed to ensure the mass conservation. The mass of the specimen is computed from the volume v^S of the specimen and from the total length l of the beams: $m^S = v^S \rho^S = \pi r^2 l \rho$.

3. The tensile failure stress of the model σ^f is obtained from dynamic tensile simulations. In this model, the material law described in subsection 2.3 is used with a huge value for yield stress in order to deactivate the plasticity (standing for buckling) that does not occur in tension. Several computation with varying values of σ^f are done until the macroscopic tensile failure stress of the specimen $\sigma^{S,tf}$ matches the value of Tab. 1.

4. The yield stress σ^y is found from dynamic crushing simulations. Several computations are launched to match the plateau stress of the specimen $\sigma^{S,y}$ due to the buckling of the edges. In this part, the contact radius r^c between the beams can also be determined to initiate the densification at the suited strain. However, since there is a lack of data for densification, in this study the contact radius r^c is simply taken equal to the true radius of the beams r.

5. Shear computations are performed to validate the identified values since this loading can be seen as a combination of tension and compression in the principal stress space.

Table 3: Properties of the model at various scales

Property	Symbol	Unit	Scales		
Edge length	a	mm	0.25	0.5	1
Minimal edge length	a_{min}	mm	0.05	0.1	0.2
Standard deviation	σ_{sd}	-	0.08	0.26	0.6
Plastic density	ρ	kg/m^3	161	158	153.5
Cross section radius	r	mm	0,075 5	0.153	0.31
Contact radius (not identified)	r^c	mm	0,075 5	0.153	0.31
Elastic modulus	E	MPa	3 000	3 000	3 000
Poisson's ratio	ν	-	0.3	0.3	0.3
Brittle tensile failure stress	σ^f	MPa	22.1	20.5	19.5
Compressive plastic yield stress	σ^y	MPa	4.7	4.7	4.7

Now that the parameters of the model are available for three investigated sizes of unit cell, the results are presented.

4 Results and discussion

In this section, the results are presented in terms of true stress versus true strain curves and degradation phenomena. Tensile, crushing and shear tests are analysed. The interest of the change in scale strategy is then discussed.

4.1 Boundary conditions

The boundary conditions are imposed to the specimens by the mean of two master nodes controlling slave nodes located at the bottom and at the top of specimen. In Tab. 2, the "tie length" b corresponds to the thickness of constrained nodes in the z direction. For example, the $72 \times 6 \times 8$ mm shear specimen has a 1 mm tie length on each side. This means that the nodes such that $z \in [0, 1]$ are tied to the bottom master node and that the nodes such that $z \in [7, 8]$ are tied to the top master node. Hence, the free height of the specimen is 6 mm. The value of b is chosen empirically to constrain enough slave nodes to impose the boundary conditions. The bottom master node is locked, whereas the top master node can only translate in one direction to induce a tensile, a compressive or a shear loading with an average macroscopic strain rate of 200 s^{-1}.

4.2 Tensile tests

The mechanical response of Rohacell specimens subjected to tensile loading are plotted in Fig. 11.

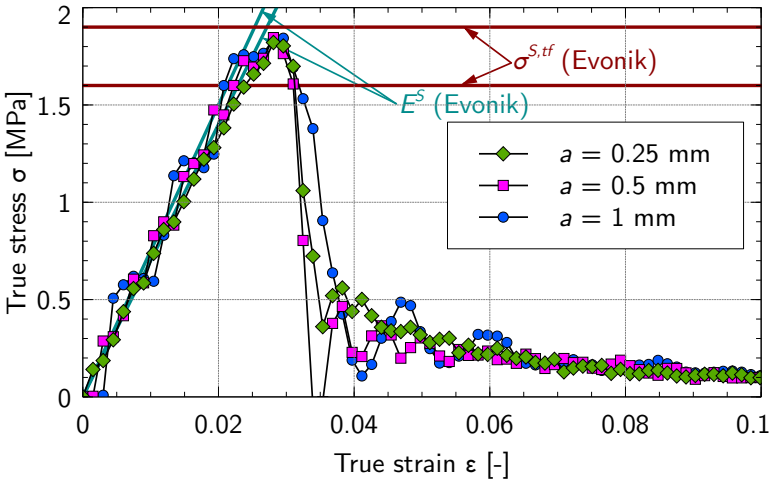

Figure 11: Tensile responses for the three unit cell sizes $a = 0.25$, 0.5 and 1 mm

The true stress versus true strain curves are in very good agreement with values available from Tab. 1 for the three investigated sizes of cells. After a linear elastic part, the brittle failure of the edges induces the failure of the specimen has illustrated in Fig. 12.

For the three specimens, a macro crack quickly propagates through the whole section leading to the brittle failure. These results match the observations made by [Christensen, Freeman and DeTeresa (2002)].

4.3 Crushing tests

The results for the crushing simulations are plotted in Fig. 13.

Here, the model shows its ability to predict both the linear elastic part and the apparition of the plateau stress due to the buckling of the edges. A similar curve is obtained for the three scale up to a strain of around 0.5. However, after this level of compaction, divergence appears between the smallest cell size specimen and the two other. This is mainly due to the lack of identification upon the contact radius r^c in the model. Extra work should be accomplished to find a proper value for this r^c

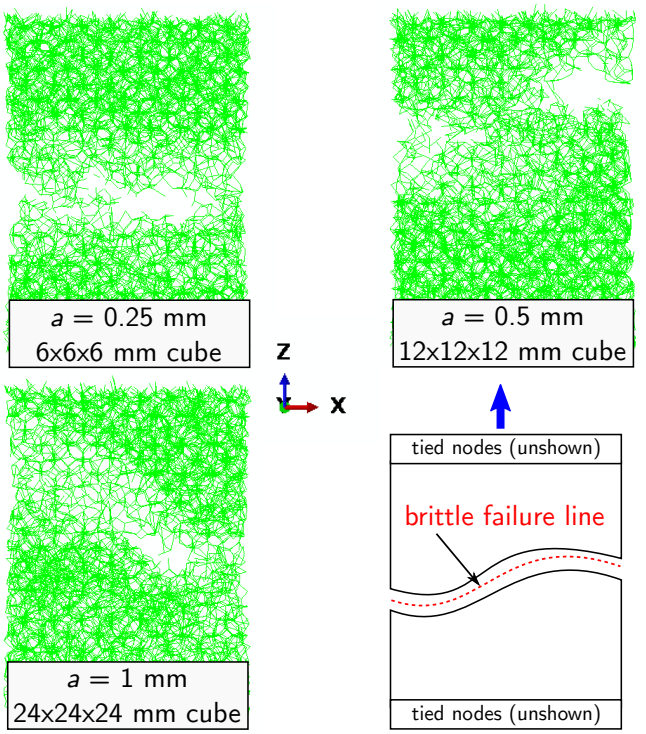

Figure 12: Tensile test for the three unit cell sizes $a = 0.25$, 0.5 and 1 mm

parameter, particularly for $a = 0.25$ mm. As the model tends to be used with bigger cell sizes, this issue does not appear critical.

The *scenario* of failure of the specimen is illustrated in Fig. 14. As it is the same for the three cell sizes, only the intermediate one of $a = 0.5$ mm is shown at several steps of loading.

At 20 % of loading, a band of edges subjected to buckling appears on the left of the specimen. This state correspond to the initiation of the plateau stress. Up to 70/80 % of loading, the band propagates through the thickness of the specimen. When the beam elements are all in contact, the densification step initiates.

Once again, the model behaviour is in good agreement with observations made by [Zhu, Mills and Knott (1997); Li, Mines and Birch (2000); Gibson and Ashby (2001); Christensen (2000); Jang and Kyriakides (2009b); Jang and Kyriakides (2009a)], even if some of these observations were made on open cells foams.

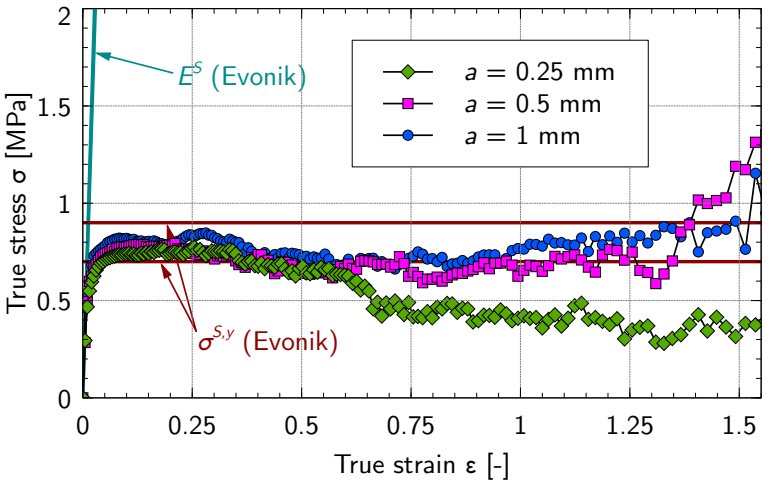

Figure 13: Crushing responses for the three unit cell sizes $a = 0.25$, 0.5 and 1 mm

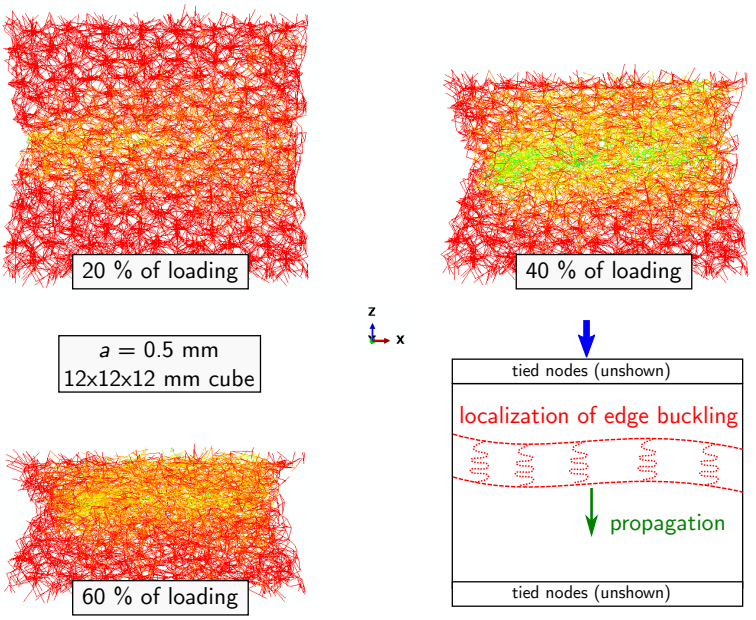

Figure 14: Crushing test of a $12 \times 12 \times 12$ mm specimen

4.4 Shear tests

The results obtained under shear loading are plotted in Fig. 15.

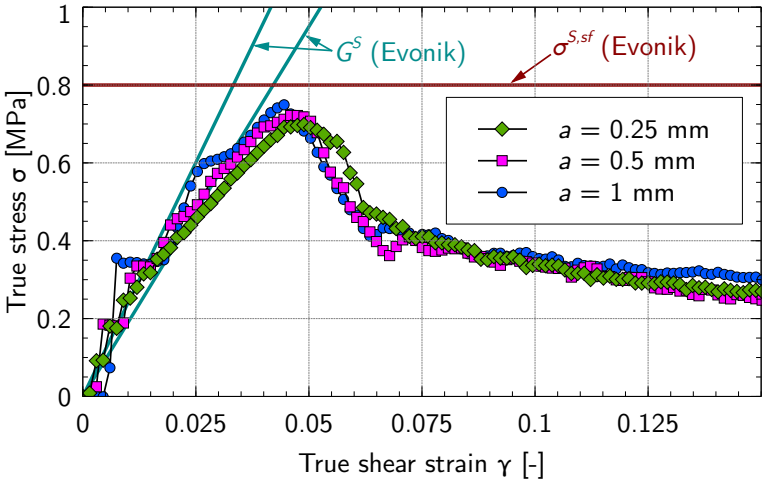

Figure 15: Shear responses of for the three unit cell sizes: $a = 0.25$, 0.5 and 1 mm

After a short linear part of satisfactory shear modulus, the stress versus strain curve exhibits a non linear shape that is due to the apparition of plasticity (buckling) in the zones subjected to compression and to the apparition of tensile failures of some edges loaded in tension. As can be seen in Fig. 16, several cracks quickly propagates in a plan perpendicular to the principal tensile stress direction. Once they meet, the specimen fails. The residual stress is due to the contact between the beam elements which induces a friction between the upper and lower parts of the broken specimen.

The failure under shear loading appears at $\sigma = 0.7$ MPa rather than at 0.8 MPa as might have been expected. This is maybe due to the perturbation process that can not ensure convex shapes for the cells of the Rohacell model. Another strategy relying on Voronoi's cell will be investigated in the future.

Apart from this last point, the model produces satisfactory load response and degradation phenomena for the three investigated scales. This validates the change in scale approach in a physical point of view.

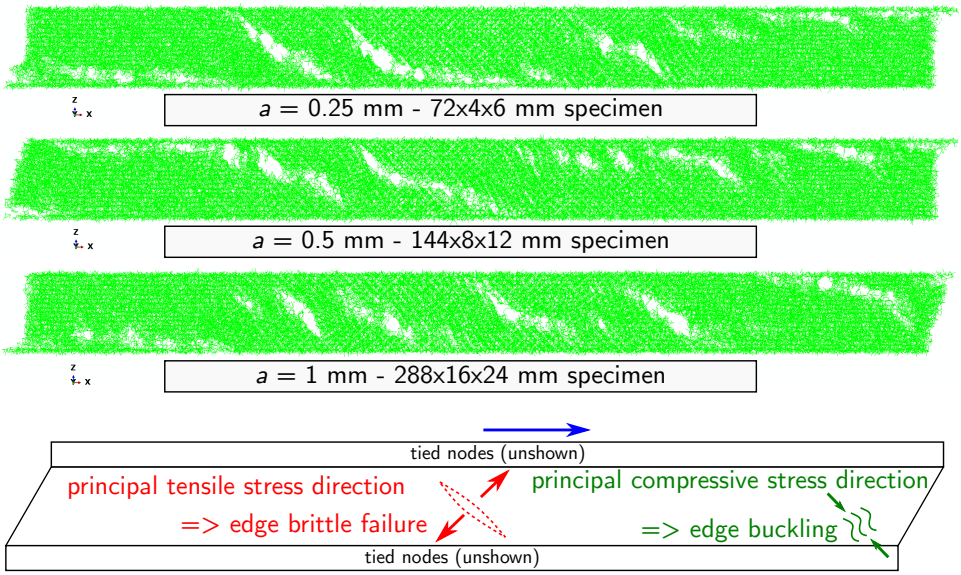

Figure 16: Shear test for the three unit cell sizes $a = 0.25$, 0.5 and 1 mm

4.5 Computational time gains

In this part a comparison between the computational times obtained for the specimens meshed with three edge lengths ($a = 0.25$, 0.5 and 1 mm), is performed. The meshed specimens are presented in Fig. 17. Unlike the identification step, where the dimensions of the specimens were chosen to preserve the number of cells regardless of the size of the microstructure, here the size of the specimens is constant so as to vary the number of cells for a given structure.

The tensile, crushing and shear loadings are simulated on a parallel computer involving 16 cores (4 processors with 4 cores per processor). A summary of the computation times obtained is available in Fig. 18.

The reference time is set to 1 for the miscrostructure with $a = 0.25$ mm. As the y axis is in log scale, it can be seen from this bar plot that the gain in time is of an order of 30 between the 0.25 and the 0.5 mm scales and of an order of 400 between the 0.25 and the 1 mm scales.

In compression, large time is needed to reach an important crushing strain. In shear the computation time is also significant but, this time, due to the high number of cells. With this loading conditions, the gains are very impressive with a reference time of more than 20 hours at 0.25 mm and of less than 3 minutes at 1 mm.

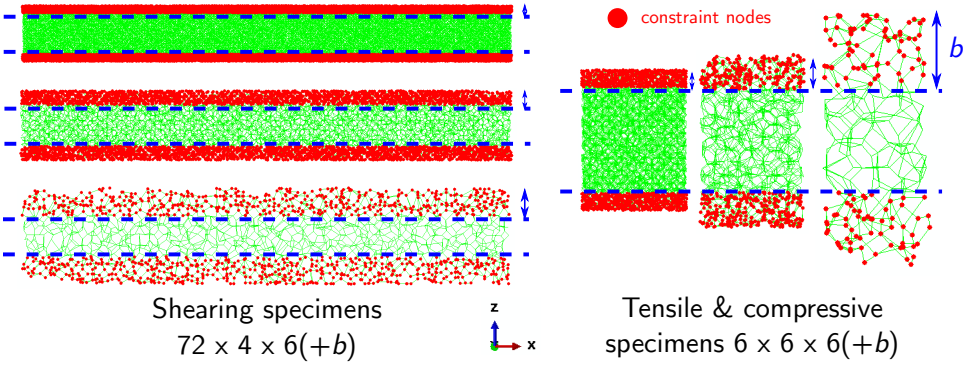

Figure 17: Specimens used for testing the influence of the cell size ($a = 0.25$, 0.5 and 1 mm) on the computational time

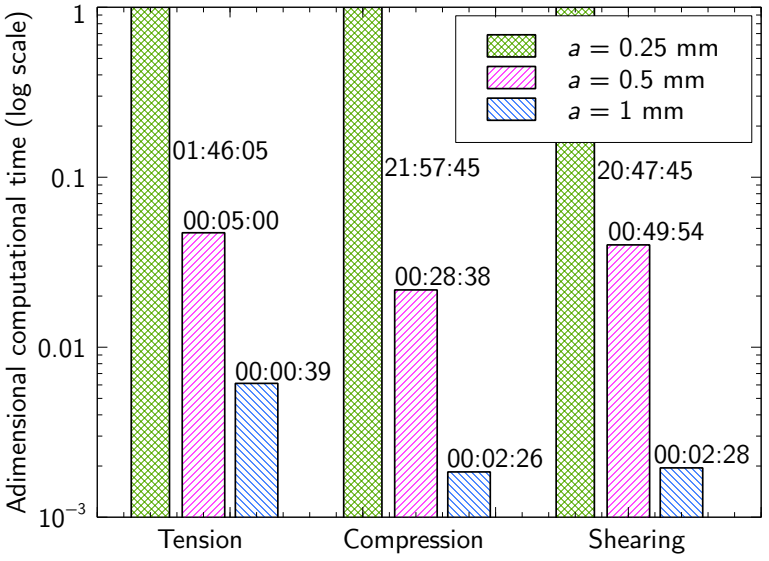

Figure 18: Computational times for $a = 0.25$, 0.5 and 1 mm

Two points can explain these results:

- for a given volume, a change by a factor 2 of the length a of the edge results in a change by a factor of 2^3 of the number of cells;

- when the edge length a of the unit cell increases, the explicit time step becomes higher, reducing the number of needed iterations.

More surprisingly, despite the small number of cells present in the specimen with the larger size of microstructure ($a = 1$ mm - see Fig. 17), the true stress versus true strain curves remain satisfactory as shown in Fig. 19.

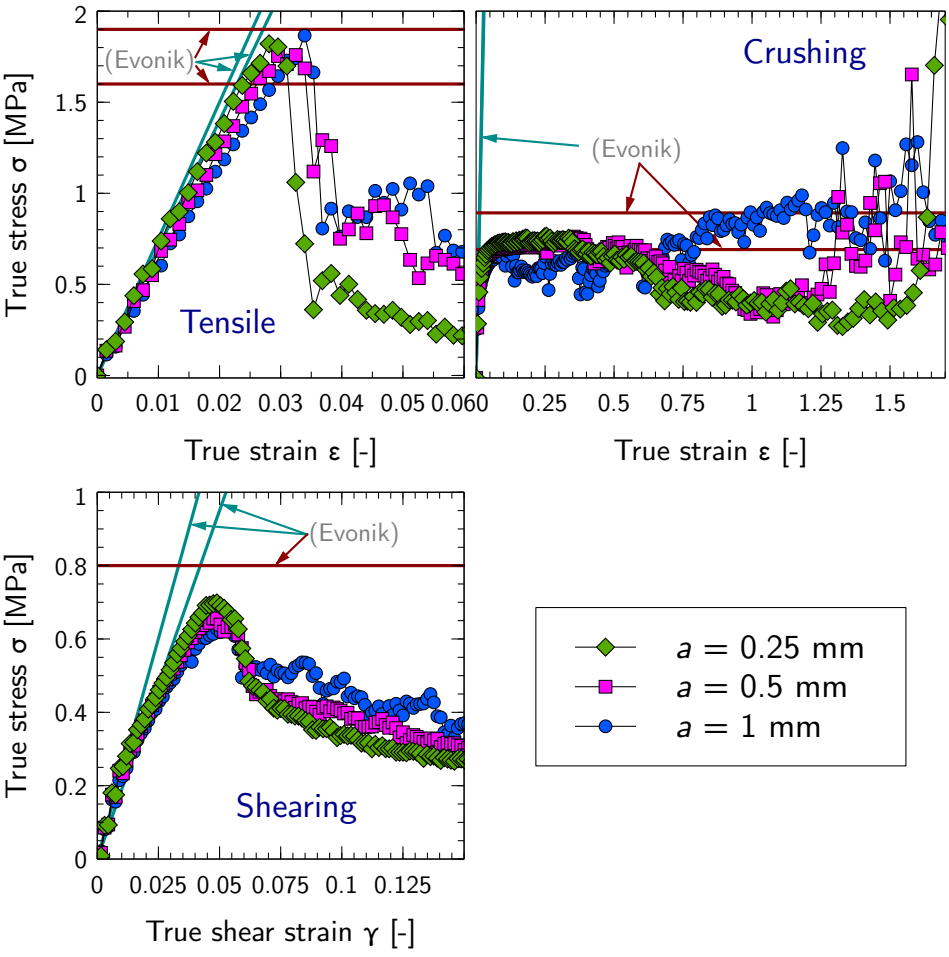

Figure 19: Tensile, crushing and shear curves for the three sizes of microstructures ($a = 0.25$, 0.5 and 1 mm) used with the $a = 0.25$ mm specimens sizes

An illustration of the damage configurations, obtained in the case of the shear loading, is presented in Fig. 20 for the three sizes of microstructure ($a = 0.25$, 0.5 and

1 mm). The brittle failure and buckling of the edges are retrieved with the three microstructures even if the description is finest for the smallest one ($a = 0.25$ mm).

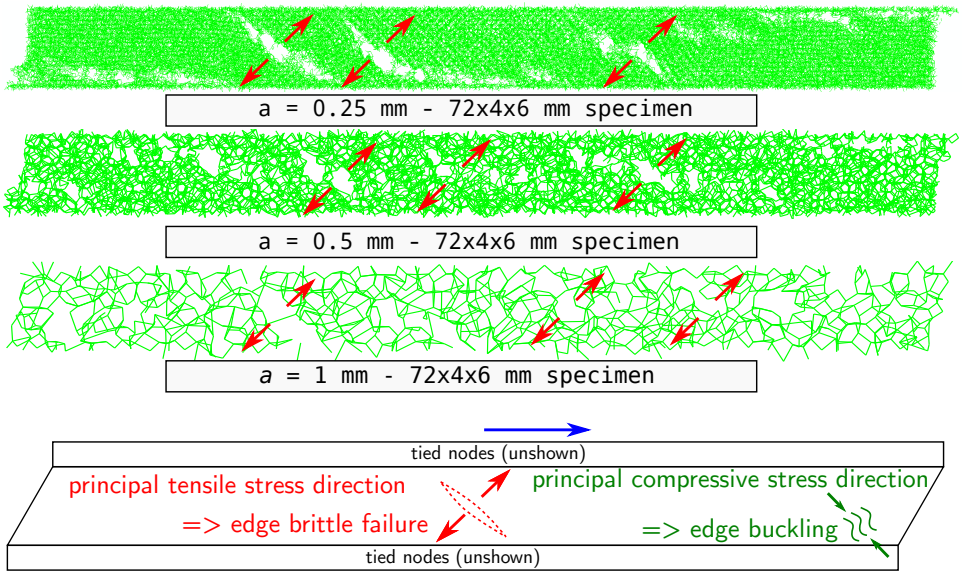

Figure 20: Damage configurations in the case of the shear loading for the three sizes of microstructures ($a = 0.25$, 0.5 and 1 mm)

With a satisfactory mechanical behaviour at each scale and a huge gain in computational time, it becomes possible to consider the simulation of large-size structures involving the modelling of the foam core material with the proposed strategy. Although no study has been conducted at larger scales than $a = 1$ mm, there is no fundamental reason that precludes the use of this approach at larger scales. The choice of a larger edge length a enables the computation of large structures but leads to a loss of details in the spatial description of the degradation phenomena, which will still appear, but more coarsely.

5 Conclusion

In this paper, a modelling strategy dedicated to Rohacell polymeric foams has been presented. It is developed in the context for the finite elements method with explicit time integration scheme to face impact loadings. The model involves several assumptions and simplifications used to make a compromise between the micro and macro scales: truncated octahedron as unit cell, beam elements to mesh the lattice

unit cell, simple perturbation process and material law. If this simple microscopic model can probably be greatly improved, it has shown a good capability to be identified at various scales in order to match experimental data. Moreover, the physical degradation phenomena are well represented at each scale. This enables a fine analysis of the degradation of the foam, even for large structures since significant computational time gains can be achieved due to the change in scale strategy.

The prospects of this study are: the improvement of the description of the microstructure as has been done by [Jang, Kraynik and Kyriakides (2008)], the introduction of the slight anisotropy due to the manufacturing process of Rohacell foams and the modelling of the strain rate effects as highlighted by [Bouix, Viot and Lataillade (2009)].

Acknowledgement: The author acknowledge with thanks Mr Laurent MIOTTO from EVONIK for its support about Rohacell foam and CALMIP (CALcul en Midi-Pyrénées) for its provision of a massively parallel computation architecture.

References

Abrate, S. (2008): Functionally graded plates behave like homogeneous plates. *Composites Part B: Engineering*, vol. 39, no. 1, pp. 151–158.

Aktay, L.; Johnson, A.; Toksoy, A.; Kröplin, B.-H.; Güden, M. (2008): Modeling the progressive axial crushing of foam-filled aluminum tubes using smooth particle hydrodynamics and coupled finite element model/smooth particle hydrodynamics. *Materials & Design*, vol. 29, no. 3, pp. 569–575.

Aktay, L.; Johnson, A. F.; Kröplin, B.-H. (2008): Numerical modelling of honeycomb core crush behaviour. *Engineering Fracture Mechanics*, vol. 75, no. 9, pp. 2616–2630.

Altair (2009): *Radioss Theory Manual*.

Aminanda, Y.; Castanié, B.; Barrau, J.-J.; Thevenet, P. (2009): Experimental and numerical study of compression after impact of sandwich structures with metallic skins. *Composites Science and Technology*, vol. 69, no. 1, pp. 50–59.

ASTM Standard (2011): Test method for shear properties of sandwich core materials. Technical report, ASTM International, 2011.

Azikri de Deus, H. P.; Alves, M. K. (2009): An application for polymer foams. In *Mechanics of Solids in Brazil*, pg. 49–67. Brazilian society of mechanical sciences and engineering edition.

Bishay, P. L.; Atluri, S. N. (2012): High-performance 3d hybrid/mixed, and simple 3d voronoi cell finite elements, for macro- &micro-mechanical modeling of

solids, without using multi-field variational principles. *CMES: Computer Modeling in Engineering & Sciences*, vol. 84, no. 1, pp. 41–97.

Bishay, P. L.; Atluri, S. N. (2013): 2d and 3d multiphysics voronoi cells, based on radial basis functions, for direct mesoscale numerical simulation (dmns) of the switching phenomena in ferroelectric polycrystalline materials. *CMC: Computers, Materials & Continua*, vol. 33, no. 1, pp. 19–62.

Bishay, P. L.; Atluri, S. N. (2014): Trefftz-lekhnitskii grains (tlgs) for efficient direct numerical simulation (dns) of the micro/meso mechanics of porous piezoelectric materials. *Computational Materials Science*, vol. 83, pp. 235–249.

Bouix, R.; Viot, P.; Lataillade, J.-L. (2009): Polypropylene foam behaviour under dynamic loadings: Strain rate, density and microstructure effects. *International Journal of Impact Engineering*, vol. 36, no. 2, pp. 329–342.

Christensen, R. (2000): Mechanics of cellular and other low-density materials. *International Journal of Solids and Structures*, vol. 37, no. 1-2, pp. 93–104.

Christensen, R. M.; Freeman, D. C.; DeTeresa, S. J. (2002): Failure criteria for isotropic materials, applications to low-density types. *International Journal of Solids and Structures*, vol. 39, no. 4, pp. 973–982.

Dong, L.; Atluri, S. N. (2012): Development of 3d t-trefftz voronoi cell finite elements with/without spherical voids &/or elastic/rigid inclusions for micromechanical modeling of heterogeneous materials. *CMC: Computers, Materials & Continua*, vol. 30, no. 2, pp. 169–212.

Dong, L.; Atluri, S. N. (2012): T-trefftz voronoi cell finite elements with elastic/rigid inclusions or voids for micromechanical analysis of composite and porous materials. *CMES: Computer Modeling in Engineering & Sciences*, vol. 83, no. 2, pp. 183–219.

Dong, L.; Atluri, S. N. (2013): Sgbem voronoi cells (svcs), with embedded arbitrary-shaped inclusions, voids, and/or cracks, for micromechanical modeling of heterogeneous materials. *CMC: Computers, Materials & Continua*, vol. 33, no. 2, pp. 111–154.

Evonik (2011): Rohacell a product information, 2011.

Gaitanaros, S.; Kyriakides, S.; Kraynik, A. M. (2012): On the crushing response of random open-cell foams. *International Journal of Solids and Structures*, vol. 49, no. 19-20, pp. 2733–2743.

Gibson, L. J.; Ashby, M. F. (2001): *Cellular solids : structure and properties*. Cambridge University Press, Cambridge.

Gibson, L. J.; Ashby, M. F.; Harley, B. A. (2010): *Cellular materials in nature and medicine*. Cambridge University Press, Cambridge ; New York.

Gong, L.; Kyriakides, S. (2005): Compressive response of open cell foams part II: initiation and evolution of crushing. *International Journal of Solids and Structures*, vol. 42, no. 5–6, pp. 1381–1399.

Gong, L.; Kyriakides, S.; Jang, W.-Y. (2005): Compressive response of open-cell foams. part i: Morphology and elastic properties. *International Journal of Solids and Structures*, vol. 42, no. 5–6, pp. 1355–1379.

Gornet, L.; Marguet, S.; Marckmann, G. (2006): Finite element modeling of Nomex® honeycomb cores : Failure and effective elastic properties. *CMC*, vol. 4, no. 2, pp. 63–74.

Jang, W.-Y.; Kraynik, A. M.; Kyriakides, S. (2008): On the microstructure of open-cell foams and its effect on elastic properties. *International Journal of Solids and Structures*, vol. 45, no. 7-8, pp. 1845–1875.

Jang, W.-Y.; Kyriakides, S. (2009): On the crushing of aluminum open-cell foams: Part i. experiments. *International Journal of Solids and Structures*, vol. 46, no. 3-4, pp. 617–634.

Jang, W.-Y.; Kyriakides, S. (2009): On the crushing of aluminum open-cell foams: Part II analysis. *International Journal of Solids and Structures*, vol. 46, no. 3-4, pp. 635–650.

Jang, W.-Y.; Kyriakides, S.; Kraynik, A. M. (2010): On the compressive strength of open-cell metal foams with kelvin and random cell structures. *International Journal of Solids and Structures*, vol. 47, no. 21, pp. 2872–2883.

Kraynik, A.; Reinelt, D.; van Swol, F. (2003): Structure of random monodisperse foam. *Physical Review E*, vol. 67, no. 3.

Laroussi, M.; Sab, K.; Alaoui, A. (2002): Foam mechanics: nonlinear response of an elastic 3D-periodic microstructure. *International Journal of Solids and Structures*, vol. 39, no. 13-14, pp. 3599–3623.

Li, Q.; Mines, R.; Birch, R. (2000): The crush behaviour of rohacell-51WF structural foam. *International Journal of Solids and Structures*, vol. 37, no. 43, pp. 6321–6341.

Navarro, P.; Aubry, J.; Marguet, S.; Ferrero, J.-F.; Lemaire, S.; Rauch, P. (2012): Experimental and numerical study of oblique impact on woven composite sandwich structure: Influence of the firing axis orientation. *Composite Structures*, vol. 94, no. 6, pp. 1967–1972.

Navarro, P.; Aubry, J.; Marguet, S.; Ferrero, J.-F.; Lemaire, S.; Rauch, P. (2012): Semi-continuous approach for the modeling of thin woven composite panels applied to oblique impacts on helicopter blades. *Composites Part A: Applied Science and Manufacturing*, vol. 43, no. 6, pp. 871–879.

Okabe, A.; Boots, B.; Sugihara, K.; Chiu, S. N. (2000): *Spatial tessellations : concepts and algorithms of Voronoi diagrams*. J. Wiley & Sons, Chichester [etc.].

Schubel, P. M.; Luo, J.-J.; Daniel, I. M. (2007): Impact and post impact behaviour of composite sandwich panels. *Composites: Part A*, vol. 38, pp. 1051–1057.

Simulia (2011): Abaqus 6.11 documentation, 2011.

Tawk, I.; Aubry, J.; Navarro, P.; Ferrero, J.-F.; Marguet, S.; Rivallant, S.; Lemaire, S.; Rauch, P. (2012): Study of impact on helicopter blade. *Engineering Failure Analysis*, vol. 24, pp. 38–45.

Thomson, W. (1887): On the division of space with minimum partitional area. *Philosophical Magazine*, vol. 24, no. 151, pp. 503.

Zhu, H.; Knott, J.; Mills, N. (1997): Analysis of the elastic properties of open-cell foams with tetrakaidecahedral cells. *Journal of the Mechanics and Physics of Solids*, vol. 45, no. 3, pp. 319–343.

Zhu, H.; Mills, N.; Knott, J. (1997): Analysis of the high strain compression of open-cell foams. *Journal of the Mechanics and Physics of Solids*, vol. 45, no. 11-12, pp. 1875–1904.